ANL-78-36

THE ROLE OF BUBBLE-SIZE EQUILIBRATION IN THE TRANSIENT BEHAVIOR OF FISSION GAS

by

E. E. Gruber

BASE TECHNOLOGY

U of C-AUA-USDOE

ARGONNE NATIONAL LABORATORY, ARGONNE, ILLINOIS

Prepared for the U. S. DEPARTMENT OF ENERGY
under Contract W-31-109-Eng-38

Printed in the United States of America
Available from
National Technical Information Service
U. S. Department of Commerce
5285 Port Royal Road
Springfield, Virginia 22161
Price: Printed Copy $4.50; Microfiche $3.00

Distribution Category:
LMFBR Safety (UC-79p)

ANL-78-36

ARGONNE NATIONAL LABORATORY
9700 South Cass Avenue
Argonne, Illinois 60439

THE ROLE OF BUBBLE-SIZE EQUILIBRATION IN THE TRANSIENT BEHAVIOR OF FISSION GAS

by

E. E. Gruber

Reactor Analysis and Safety Division

April 1978

TABLE OF CONTENTS

LIST OF FIGURES

LIST OF TABLES

THE ROLE OF BUBBLE-SIZE EQUILIBRATION IN THE TRANSIENT BEHAVIOR OF FISSION GAS

by

E. E. Gruber

ABSTRACT

An explicit analysis of bubble-size equilibration by volume diffusion has been derived and incorporated into the FRAS2 code. This code was developed for mechanistic analysis of transient fission-gas behavior in LMFBR fuel, but had been limited by the approximation that the time required for bubble-size adjustment, following coalescence or changes in temperature or pressure, was negligible.

The equilibration phenomenon is illustrated by several idealized examples. If the fuel temperature rises linearly with time, an isolated bubble will expand rapidly toward its equilibrium size only after the temperature reaches a critical value that depends on both bubble size and heating rate. Conversely, if the temperature is reduced uniformly, an isolated bubble will shrink only until diffusion becomes too slow for further size change. The final size that is "frozen in" may be significantly larger than the final equilibrium size. Finally, isothermal equilibration following coalescence of two equal bubbles can be described conveniently in terms of relaxation times, which depend on bubble size and temperature.

However, a complete picture of the role of equilibration in transient fission-gas behavior can only be gained through an investigation of the bubble-size distribution and its evolution. Such an investigation is carried out with the FRAS2 code, in which the explicit equilibration model is implemented. Since nonequilibrium bubbles in a thermal transient are generally overpressured, the gas represents a source of energy that can conceivably disrupt the fuel. This "dispersive potential" is also calculated in the FRAS2 code.

I. INTRODUCTION

Migration and coalescence of fission-gas bubbles are important phenomena in the transient behavior of nuclear fuels. An understanding of these fundamental processes is essential to develop useful treatments of the effects of fission gas on fuel swelling and disruption during thermal transients.

Since both migration and coalescence rates depend on bubble size, it is necessary to characterize this size accurately in modeling calculations. In most analyses, the bubble radius r is assumed to satisfy the equilibrium relation $r = 2\gamma/(p - p_h)$, where γ is the surface tension and $p - p_h$ is the excess pressure in the bubble compared to the hydrostatic stress in the surrounding medium.

When two bubbles coalesce, however, two distinct processes occur, essentially consecutively. First, there is a conversion from a double-bubble configuration to a larger single bubble with the same total volume. This step occurs, in the case of small bubbles ($r \lesssim 1$ μm), primarily by the surface-diffusion migration of atoms driven by capillarity effects. Other mechanisms could also contribute to this morphology change, depending on conditions: volume diffusion, evaporation-condensation, and even viscous flow or creep. The initial result of this first step is a spherical bubble of the same volume as the initial bubble pair. Nichols[1] has shown that the driving force for this step is the decrease in surface energy because of the net reduction in surface area, and that coalescence should occur for all practical cases.

The second process is one of volume adjustment. Since for instantaneous coalescence the gas pressure is unchanged, while r is increased, the surface-tension restraint $2\gamma/r$ is not sufficient to balance the gas pressure, and the bubble will tend to expand. This expansion must take place by long-range migration of atoms or volume diffusion (although creep may contribute in some cases). The process of volume adjustment is always thermodynamically favorable and is driven by the free energy change of the gas within the bubble. Nichols has pointed out, however, that volume adjustment is much slower than coalescence, because of both a lower driving force and a slower transport mechanism. This difference in rates, in fact, is the feature that makes it convenient to consider coalescence and size adjustment as occurring consecutively, rather than simultaneously.

These considerations were at least qualitatively recognized even before Nichols' analysis. However, because of the difficulty in incorporating the volume-equilibration process into modeling of fission-gas behavior, it has generally been assumed that coalescence and equilibration both occur instantaneously.[2,3] This assumption has come into question recently as modeling efforts have matured and as the experimental data base has broadened.

The general effect of nonequilibrium on transient fission-gas behavior is qualitatively simple: the bubbles do not expand as rapidly as predicted by instantaneous equilibration models when temperature increases, pressure decreases, or coalescence occurs. As a result, the bubbles migrate faster, causing enhanced release, and contribute less to swelling. A quantitative assessment is not so simple, however. Coalescence probabilities also depend on bubble sizes, both through the effect on migration velocity or diffusivity, and through the effect on the cross sections for collisional coalescence.

In an attempt to include equilibration effects in the modeling of transient fission-gas behavior, Esteves[4] developed a two-variable multigroup numerical approximation to describe the evolution of the bubble population. This work was extended by others,[5] and applied to determine the importance of nonequilibrium bubbles. A small but significant enhancement of fission-gas release for the TREAT H3 transient[6] was predicted by the calculations. Other features that were predicted included a "freezing in" of the bubble-size distribution during cooling and a reduction in swelling. The detailed two-variable treatment, however, leads to increased complexity and computer storage requirements.

The steady-state GRASS code also treats bubbles as growing to equilibrium size instantaneously following coalescence. When GRASS results were compared to experimental data, it was found that a modification was needed to describe the limited rate of growth of coalescing bubbles. In an effort to keep computational requirements small, a simple modification was developed by J. Rest.[7] The rate at which bubbles grow from the i to the i + 1 class is now reduced from the calculated rate by a relaxation-time factor, which depends on the bubble size as well as the energies of formation and migration of vacancies.

C. Ronchi suggested a more comprehensive procedure by which the rate of growth of nonequilibrium bubbles could be included explicitly in transient calculations with the GRASS code.[8] That analysis, which apparently has not

been implemented, is based on the assumption that the force on a vacancy depends on the variation in the radial stress component with distance from the bubble.

In another analysis of the equilibration phenomenon, W. Wang and R. Singh have analyzed equilibration by primary creep.[9] Vacancy diffusion was also considered in their work, but the driving force for vacancy diffusion was considered to be the equivalent stress at the bubble surface.

If equilibration were assumed to result from vacancy diffusion caused by stress effects, the most plausible driving force for vacancy diffusion would be the variation in hydrostatic stress with distance from the bubble. However, for an elastic continuum, the hydrostatic stress does not vary with distance from a bubble. The modification to the FRAS code[3] is not based on stress considerations. Instead, vacancy diffusion is considered to result from concentration gradients that develop around bubbles. The thermodynamic approach is used to establish boundary conditions, following Greenwood et al.[10] Minimization of the free energy change with respect to changes in bubble radius provides the equilibrium condition. The apparent driving force for equilibration that results can be expressed in terms of pressures, but does not derive from a mechanical analysis.

The motivation for the development of this treatment and its incorporation into the FRAS2 code[11] arose from the results of comparisons of experimental data with FRAS-code predictions. The experimental data included results from direct-electrical-heating (DEH) tests[12] and from FGR tests.[13] Although good agreement was obtained with the FRAS code in some cases, the bubble size was greatly overpredicted in others. In particular, it appeared that the discrepancy was greatest for rapid transients for which large bubbles were predicted, and was a direct consequence of ignoring the equilibration time in the calculations.[11]

The equilibration treatment applied in FRAS2 was developed as a compromise; equilibration is calculated explicitly, as in the work by Esteves,[4] but only an average "nonequilibrium" is considered for each size class. The explicit modeling is accomplished by assuming that coalescence initially conserves volume and that equilibration in each size class proceeds at a rate determined by volume diffusion. The modeling approach will be described in the next section. The difference between the actual and equlibrium bubble sizes can be calculated to show in detail the effects of nonequlibrium on the evolution of

the bubble-size distribution, on release of gas from the grains to grain boundaries, and on intragranular swelling. These results will be described in Sect. III.

II. ANALYSIS

A. Rate of Bubble-size Equilibration

The basic analysis of the rate at which the bubble volume changes was given in an early paper in the field of bubble physics.[10] The expression derived for the vacancy concentration at equilibrium near a bubble surface, based on free energy considerations, is

$$c^v = c_e^v \exp\left\{-[p - (2\gamma/r)]\Omega/kT\right\} . \tag{1}$$

where c_e^v is the equilibrium vacancy concentration, Ω is the molecular volume of the solid, k is Boltzmann's constant, and T is the absolute temperature. The temperature of the gas is assumed to be the same as the fuel temperature. The diffusion equation in spherical coordinates:

$$\frac{d^2c^v}{d\rho^2} + \frac{2}{\rho}\frac{dc^v}{d\rho} = 0 , \tag{2}$$

was solved to determine the vacancy flux at the bubble surface, $\rho = r$, and hence the rate of change of bubble radius. Arguments concerning fission vacancies and interstitials were introduced, but their contributions were considered small in deriving the end result:

$$\frac{dr}{dt} = D_v c_e^v \left(p - \frac{2\gamma}{r}\right)\frac{\Omega}{rkT} , \tag{3}$$

where D_v is the vacancy diffusion coefficient. Several assumptions were made in the derivation of Eq. (3). First, the exponential in Eq. (1) was assumed to be small. Second, the bubble separation 2R was assumed to be much greater than the bubble radius r. Finally, the vacancy concentration at R was taken to be the equilibrium concentration.

A more general expression that includes the effect of local hydrostatic pressure and the effect of bubble separation, and does not use an approximation for the exponential, has been derived for the present application:

$$\frac{dr}{dt} = D_u \frac{R}{r(R - r)}\left\{1 - \exp\left[-\left(p - p_h - \frac{2\gamma}{r}\right)\frac{\Omega}{kT}\right]\right\} , \tag{4}$$

where D_u has been substituted for $D_v c_e^v$, since uranium self-diffusion is rate-controlling. The correlation coefficient is taken to be unity for the present.

There is one difficulty with Eq. (4) that must be considered. As the bubble separation decreases, the equilibrium rate appears to increase. The reason for this is the assumed boundary condition that the equilibrium vacancy concentration is maintained at R even when R - r becomes very small. A more realistic equation results from the simplification used by Greenwood et al.[10] based on the assumption that R >> r. The physical implication is that the gradient in vacancy concentration at the bubble surface is the same as it would be if the bubbles were widely separated. The vacancy concentration between close, nonequilibrium bubbles would consequently be reduced from the equilibrium value. The general result is then

$$\frac{dr}{dt} = \frac{D_u}{r}\left\{1 - \exp\left[-\left(p - p_h - \frac{2\gamma}{r}\right)\frac{\Omega}{rT}\right]\right\}. \qquad (5)$$

The degree of nonequilibrium is indicated by the term in parentheses in this equation. When a bubble is formed by the coalescence of two bubbles of equal radius r, the radius increases very quickly to $2^{1/3}r$; dr/dt is then positive. Similarly, if the temperature rises, p increases, and again dr/dt is positive. A decrease in hydrostatic pressure has the same effect.

B. Relative Importance of Equilibration

Although it is difficult to characterize the conditions under which equilibration is important, some simple illustrations can be given as an aid to understanding the phenomenon. The more general application of the analysis, in the FRAS2 code, will be considered in the next subsection.

Consider first a constant-temperature ramp: dT/dt = A. An equilibrium bubble at some initial temperature, say 100 K, will tend to expand as the temperature rises. However, the rate of expansion will be negligibly small until the temperature is high enough for rapid diffusion. A simple computer program was developed to apply Eq. (5), with material properties for mixed oxide and $p_h = 0$, to this situation, using finite-difference methods. The bubble size is plotted in Fig. 1 for an initial bubble radius of 10 nm, and in Fig. 2 for an initial radius of 100 nm, as functions of temperature for temperature up to the solidus of mixed-oxide fuel. In both figures, the equilibrium

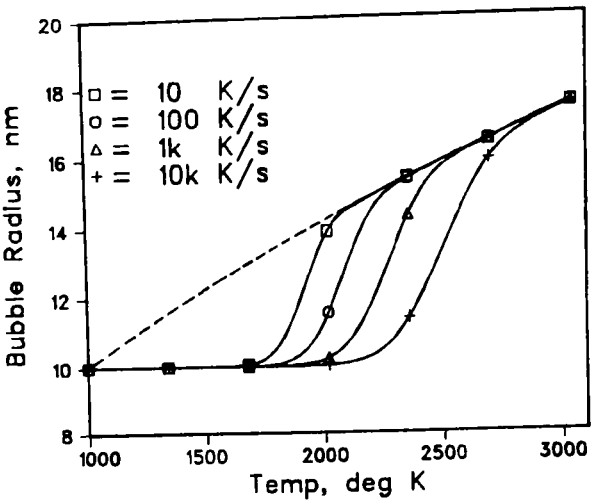

Fig. 1.
Expansion of a 10-nm Bubble for Various Thermal Ramps.

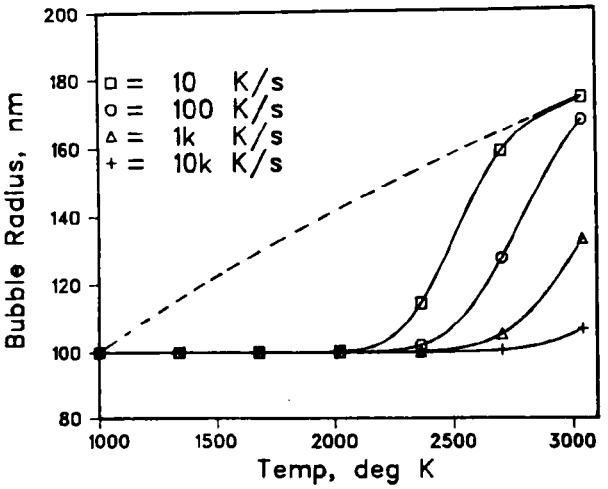

Fig. 2.
Expansion of a 100-nm Bubble for Various Thermal Ramps.

bubble radius is shown by a dashed line, and the calculated radius dependence is shown for several thermal ramp rates. The results show a very rapid expansion occurring near a critical temperature that depends on heating rate and on bubble size.

A related phenomenon is the "freezing in" of bubble sizes during cooling, discussed by Greisemeyer et al.[5] This same analysis has been applied for negative temperature ramps to study bubble shrinkage during cooling. The results are shown in Fig. 3 for a 10-nm initial bubble radius, and in Fig. 4 for a 100-nm bubble. At high temperatures, equilibrium is maintained, but as the temperature decreases, as asymptotic size is attained that depends, again, on cooling rate and initial bubble size. This size can also be characterized

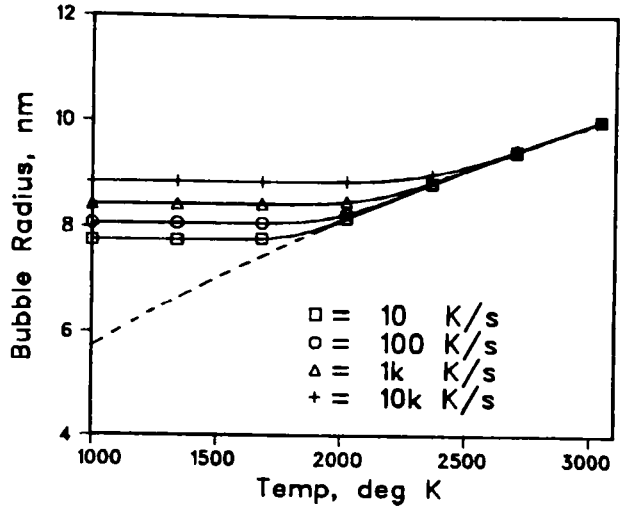

Fig. 3.
Shrinkage of a 10-nm Bubble for Various Cooling Rates.

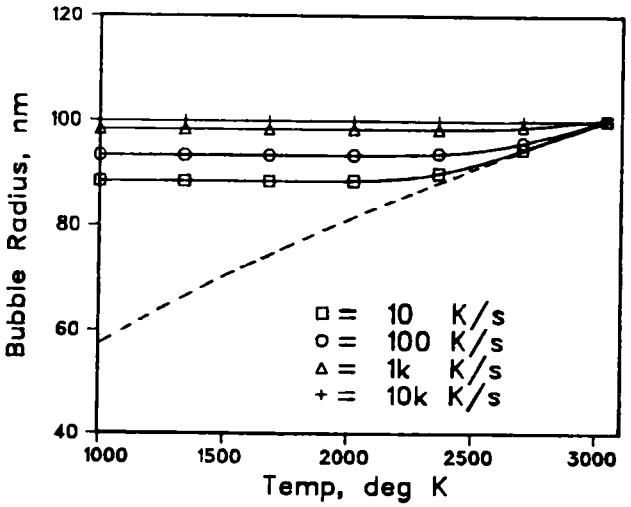

Fig. 4.
Shrinkage of a 100-nm Bubble for Various Cooling Rates.

by a critical temperature, as was done by Greisemeyer et al. for a more general distribution of bubble sizes. The fact that the "critical temperature" is only an approximation when a range of bubble sizes is considered was not noted by Greisemeyer et al., but is apparent from a comparison of Figs. 3 and 4.

The preceding discussion gives some indication of the dominance of diffusion kinetics in bubble equilibration for an isolated bubble. Another important situation is the equilibration of the product bubble formed by the coalescence of two smaller bubbles. This situation can also be treated in a simplified way to develop an understanding of the conditions for which equilibration is important.

The relaxation-time concept provides a convenient, quantitative description of the effects of the parameters involved in equilibration. An exponential decay of some parameter with time is implied in the definition of a relaxation time τ. The process considered here is the variation of the radius of a product bubble formed at $t = 0$ by the coalescence of two identical bubbles of radius r_i. The product-bubble radius r varies from an initial value r_o toward an asymptotic value r_{eq}. If the equilibration were a true exponential decay, the variation in r would be described by

$$r = r_o + (r_{eq} - r_o)(1 - e^{-t/\tau}) \quad . \tag{6}$$

Differentiation of Eq. (6) gives

$$\frac{dr}{dt} = \frac{r_{eq} - r_o}{\tau} e^{-t/\tau} \quad . \tag{7}$$

The relaxation time τ can consequently be defined from the initial slope, by setting $t = 0$ in Eq. (7) and solving for τ:

$$\tau = \frac{r_{eq} - r_o}{(dr/dt)_{t = 0}} \quad . \tag{8}$$

The actual variation of r is described by Eq. (4), which can be simplified for the present purpose by assuming that $p_h = 0$ and that the gas is ideal. The simplified form of Eq. (4) then becomes

$$\frac{dr}{dt} = \frac{D_u}{r} \left\{ 1 - \exp \left[- \frac{4\gamma\Omega}{rkT} ((r_i/r)^2 - 0.5) \right] \right\} \quad . \tag{9}$$

Although Eq. (9) is hardly of the same form as Eq. (7), the variation of r with t will be shown to be very similar to that described by Eq. (7).

Equation (9) can be simplified further by noting that, for $\gamma = 0.626$ J/m^2, $\Omega = 4.08 \times 10^{-20}$ mm^3, and $T = 2300$ K, we have $4\gamma\Omega/kT = 3.23$ nm. Since the variation of $(r_i/r)^2$ ranges from 0.5 to 0.63, it follows that, for $r \gtrsim 4$ nm, the exponential factor is $\lesssim 0.1$. Expansion of the exponential and neglect of higher-order terms yields the approximate result

$$\frac{dr}{dt} = \frac{4D_u\gamma\Omega}{r^4 kT} (r_i^2 - 0.5\, r^2) \quad . \tag{10}$$

At $t = 0$, we find $r = 1.2599\ r_i$; the initial slope is therefore

$$\left(\frac{dr}{dt}\right)_{t=0} \cong \frac{0.3275\gamma\Omega D_u}{r_i^2 kT} \quad . \tag{11}$$

From this result and the definition of τ in Eq. (8) we obtain the general result

$$\tau \cong 0.471\ r_i^3 kT/\gamma\Omega D_u \quad . \tag{12}$$

Equation (12) can be applied to quantitative examples by substituting the material parameters mentioned above and the self-diffusion coefficient[14]

$$D_u = 1.9927\ \exp(-55600/T)\ mm^2/s \tag{13}$$

to obtain

$$\tau \cong 1.275 \times 10^{-18}\ r_i^3 T\ \exp(55600/T)\ s \quad . \tag{14}$$

A simple finite-difference approach was used to solve Eq. (9) for the bubble radius as a function of time, using $T = 2273$ K and $r = 10$ nm. The results are represented in Fig. 5 by the symbols.

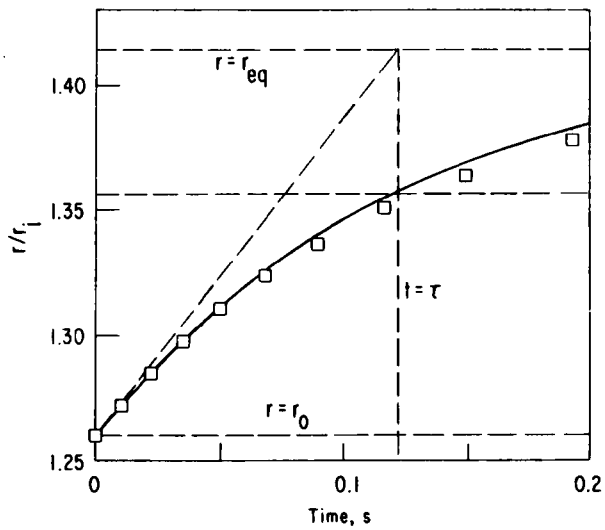

Fig. 5. Bubble Equilibration Following Coalescence of Two 10-nm Bubbles at 2273 K.

A normalized form of Eq. (6):

$$r/r_i = 1.2599 + 0.1543\ (1 - e^{-t/\tau})\ , \tag{15}$$

was also solved for the same example, using $\tau = 0.1216$ s, calculated from Eq. (14). The results are shown by the solid line in Fig. 5. At $t = \tau$, the difference between r and r_{eq} has decayed to 1/e times the initial difference. The discrepancy in the results by the two methods is small; the use of the initial slope from Eq. (11) to define the relaxation time is therefore a good approximation.

Equation (14) has been applied to a range of conditions to demonstrate the influences of bubble radius and temperature on relaxation time. The results, shown in Fig. 6, indicate that smaller bubbles should equilibrate quickly at sufficiently high temperatures. However, problems arise in transient modeling when gas concentrations are sufficiently high that the mean bubble size (and therefore the fuel swelling) becomes large. Larger bubbles may require a relaxation time significant in comparison to the transient time scale. Since bubbles may not reach equilibrium before again coalescing, subsequent product bubbles may deviate further from equilibrium. These more complex considerations are better analyzed in the more general context of the FRAS code.

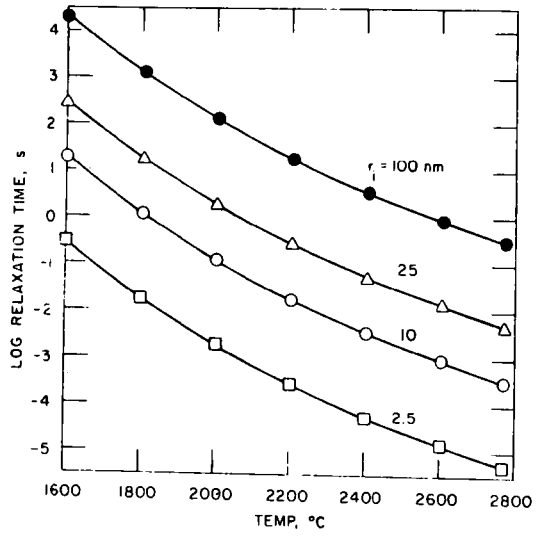

Fig. 6. Relaxation Times for Coalescence-product Bubbles as Functions of Temperature.

C. Incorporation of Equilibration in the FRAS Code

Consideration of the above discussion of equilibration effects leads to the conclusion that a general treatment is complicated. Temperature, pressure, coalescence, and bubble sizes must all be considered. Since the analysis carried out by the FRAS code includes all of these factors,[15] it is a logical step to incorporate equilibration explicitly into the code.

This step is conceptually simple, although its accomplishment in the code required extensive revision. The method can be summarized by the following steps: (1) Migration and coalescence are calculated as before, except that the nonequilibrium bubble size is used to calculate migration velocity and coalescence probability. (2) Volume is conserved upon coalescence. The volume per bubble is averaged over all bubbles in each size class. (3) All bubbles in each class are assumed to equilibrate at the same rate, determined by the average conditions in the class.

Separation of the coalescence and equilibration steps requires some justification, since both occur simultaneously in each time step. The time step is selected internally in a manner that precludes a large change in the population of a given size class in one time step. The average degree of nonequilibrium of any size class is therefore not significantly altered by coalescence in a time step, and most of the bubbles in a given class are affected only by equilibration during the step. It is therefore appropriate to evaluate the equilibration continuously over each time step. The validity of this approach is supported by preliminary analyses that indicate no significant effect of time-step size within the normal range of sizes.

A more important limitation enters in the assumption that the degree of nonequilibrium in each size class can be adequately represented by the average volume per bubble. Each size class is characterized by the mean number of gas atoms per bubble. Each coalescence results in the loss of two bubbles, with their associated numbers of gas atoms and bubble volumes, from their size classes, and the addition of one bubble, containing the same total number of gas atoms and bubble volume, to a product-bubble class. In practice, the product bubble is split fractionally between two adjacent classes so that both gas atoms and bubble numbers can be properly conserved. This procedure is necessary because only a finite number of size classes is chosen. The product bubble rarely contains the exact number of atoms used to represent a size class and will generally contribute less than the average volume per bubble in its new size class. Nevertheless, the volumes of added bubbles are averaged with the volumes of existing bubbles in the size class, to provide an average volume per bubble, from which a new, nonequilibrium, average radius is calculated for the size class.

The equilibration is calculated for each time step and size class according to Eq. (5), using a simple finite-difference treatment. The coalescence time step is subdivided as needed for the equilibration calculations. Some error is undoubtedly introduced by this procedure, but that error is difficult to quantify. The approximation is presumed to provide an effective compromise between the limitations of the unmodified FRAS code and the complexity of a multivariate analysis, such as that of Esteves.[4]

The modified code, called FRAS2, has been applied in several analyses to determine whether the results are consistent with experiments, and whether the detailed response of bubble distributions to thermal transients is as anticipated. Results of these analyses are presented in the next section.

III. RESULTS OF FRAS2 ANALYSES

A. Equilibration Effects in the H3 Transient

A series of calculations has been carried out to illustrate the effects of equilibration for the TREAT H3 transient,[6] which was analyzed in the original calibration of the FRAS code.[15] Figure 7 shows the results of four calculations

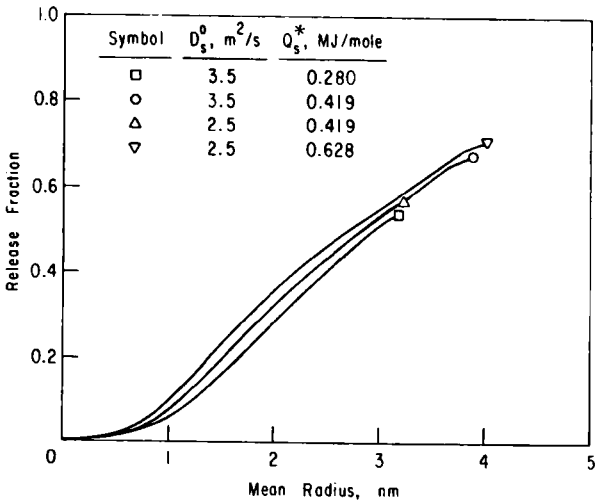

Fig. 7. FRAS Results for the TREAT H3 Test, Assuming Different Surface-diffusion Coefficients and Heats of Transport.

with the FRAS code (assuming equilibrium bubbles) for two values of the surface-diffusion pre-exponent D_s^o and three values of the heat of transport Q_s^*. The release fraction is plotted as a function of the mean bubble radius. A parametric analysis based on FRAS results has indicated a close relationship between the mean radius and the migration distance, which determines the release fraction.[16] This relationship varies slightly as the FRAS input parameters are varied, but only within a narrow range, as illustrated by Fig. 7. When Q_s^* is increased, the curve shifts slightly toward higher release fractions. When D_s^o is increased, however, the curve simply extends further along the same path.

Present information from the H3 posttest examination indicates a mean bubble radius of about 32.5 nm and a release fraction of about 0.8 for the radial node considered here.[6] This set of values corresponds to a point that would lie above the curve in Fig. 7. (The discrepancy from the original calibration of the FRAS code results from a more realistic value for grain size in the current version). Although these numbers are limited in accuracy,[17] the discrepancy appears to be significant.

Since a possible source of disagreement is the equilibration time, the FRAS2 code was used to calculate the gas release and mean radius as functions of time. The pre-exponent of the volume-diffusion coefficient was varied by a factor of 10 higher and lower than the nominal value [Eq. (13)] for these calculations. The results are shown in Fig. 8.

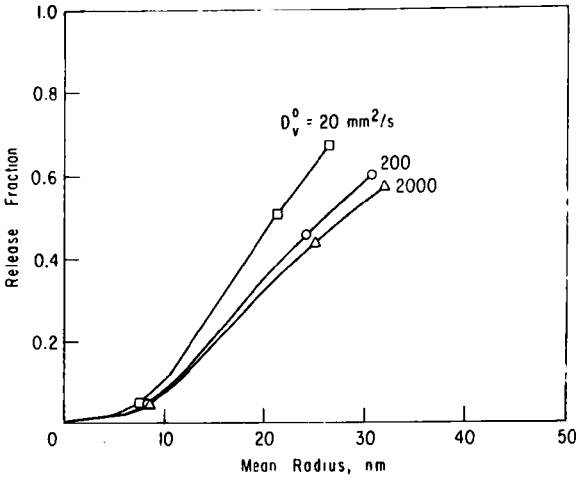

Fig. 8.
FRAS2 Results for the TREAT H3 Test, Assuming Different Volume-diffusion Coefficients.

The higher value gives complete equilibration throughout this transient, which involves fairly small bubbles. The results agree very closely with the corresponding curve in Fig. 7. The nominal and lower values result in non-equilibrium bubbles early in the transient. Release is enhanced for a given mean bubble size in these cases.

These results indicate that, for this particular set of conditions, the predicted equilibration behavior is in general agreement with the experimental results. Since the role of equilibration is relatively small here, because the mean intragranular bubble size is small and equilibration is rapid, the effects are not strong enough to provide a quantitative benchmark test for the equilibration analysis of the FRAS2 code. However, the results of this comparison provide at least qualitative support for the need for, and the validity of, the analysis.

B. Effects of Equilibration on Gas Behavior

The basic difference between the results calculated with the FRAS2 code and the results from the equilibrium analysis with the FRAS code can best be demonstrated by examining the differences in the predicted bubble-size distributions. It is expected that:

(1) the distribution will be narrower, since larger bubbles will not be able to equilibrate rapidly;

(2) there will be more release of gas to grain boundaries, since, in general, bubbles will be smaller, and hence more mobile;

(3) intragranular swelling will be reduced, because of the finite rate of bubble growth; and

(4) there will be more, smaller intragranular bubbles, since coalescence probabilities will be reduced.

In each of these areas, the effect of equilibration must be determined quantitatively. A number of variables are important in quantifying these effects, including transient period, initial gas concentration, grain size, thermal gradient, and hydrostatic pressure. Only the first of these effects is considered here.

A series of calculations was carried out to illustrate the effect of the heating rate on the bubble-size distribution, on gas release to grain boundaries, and on intragranular swelling. Heating rates of 50, 500, and 5000 K/s were considered, with other variables held constant. The values used were: grain size, 10 μm (mean linear intercept); initial gas concentration, 1 x 10^{17} atoms/mm^3; initial temperature, 1500 K; final temperature, 3040 K; thermal gradient, 500 K/mm; and pressure, 0.25 MPa.

Figure 9 shows the end-of-transient cumulative bubble-size distributions for all six calculations. Logarithmic axes are used to cover the broad range

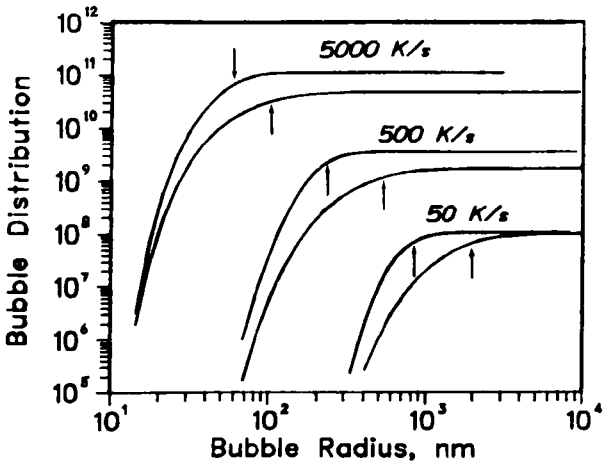

Fig. 9.
Comparison of Cumulative Bubble-size Distributions at the Solidus for Three Linear Thermal Ramps, Using FRAS and FRAS2.

of values predicted. Each distribution represents the number of bubbles per mm^3 smaller than a particular radius. Several features are apparent from

this figure: (1) There is a difference in bubble density between FRAS and FRAS2 predictions that increases with the ramp rate; (2) the mean radius, denoted by small vertical arrows in Fig. 9, is reduced by about a factor of 2 when equilibration is included; and (3) the FRAS distributions are broader than the FRAS2 distributions. Values of the bubble density and mean radius are tabulated in Table 1.

Table 1. Results of Heating-rate Comparisons

Ramp Rate, K/s	Bubble Density, Number/mm^3		Mean Radius, nm		Release, %		Peak Swelling, %	
	FRAS	FRAS2	FRAS	FRAS2	FRAS	FRAS2	FRAS	FRAS2
50	1.0×10^8	1.1×10^8	1930	825	70.4	100.0	221	6.8
500	1.7×10^9	3.5×10^9	524	234	32.6	62.9	198	10.6
5000	4.6×10^{10}	1.1×10^{11}	106	61	15.0	21.7	66	10.9

A linear plot of the FRAS and FRAS2 results for the 500 K/s thermal ramp is provided in Fig. 10. These distributions are very similar in shape, although

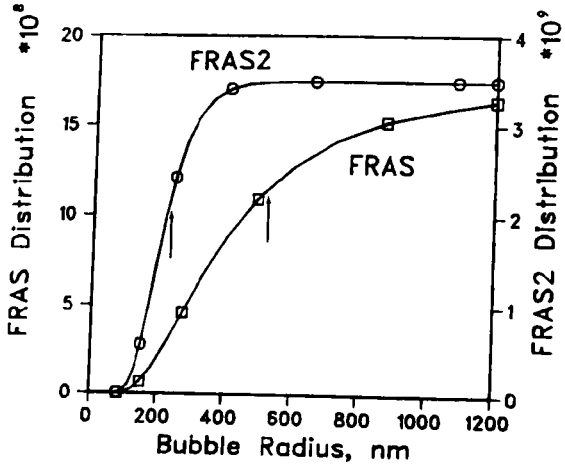

Fig. 10. Cumulative Bubble-size Distributions Calculated with the FRAS and FRAS2 Codes for a 500-K/s Heating Rate.

not in magnitude, to those calculated for the other thermal ramps. The FRAS2 distribution is much narrower, with about the same minimum bubble size, but none of the larger bubbles predicted by the FRAS calculation.

The vertical arrows in Fig. 10 indicate the mean radii for the two calculations. The FRAS2 calculation predicts a mean radius less than half that predicted in the FRAS calculation. As a consequence, the gas release to grain boundaries is increased by nearly a factor of two. Table 1 includes gas-release results at transient termination for the three ramps.

More detailed results of gas-release calculations are shown in Fig. 11 for FRAS calculations and in Fig. 12 for FRAS2 calculations. In both cases,

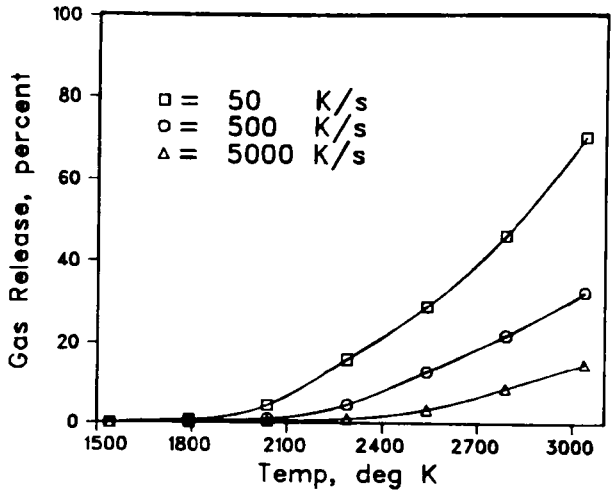

Fig. 11.
Gas Release to Grain Boundaries for Three Heating Rates, Calculated with the FRAS Code.

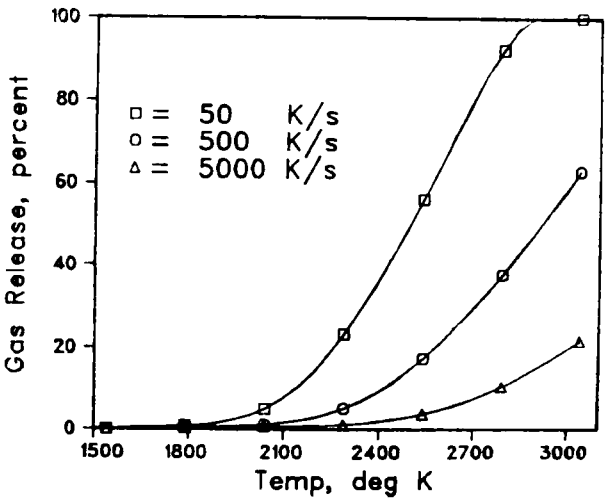

Fig. 12.
Gas Release to Grain Boundaries for Three Heating Rates, Calculated with the FRAS2 Code.

increasing the rate of temperature rise reduces the gas-release rate. The gas release calculated by the two codes is very similar up to about 5% release, which corresponds roughly to a mean bubble radius of 15 nm. The curves subsequently diverge, with the least effect being seen for the fastest thermal ramp, corresponding to the smallest mean bubble sizes. Again, it is apparent that nonequilibrium effects are greater for larger bubbles.

Peak values of intragranular swelling are also listed in Table 1. The major result is the large effect of absence of equilibrium, which reduces the peak swelling by a factor of 30 in the slowest transient. More detailed results are shown in Fig. 13 for the FRAS calculations. Swelling decreases

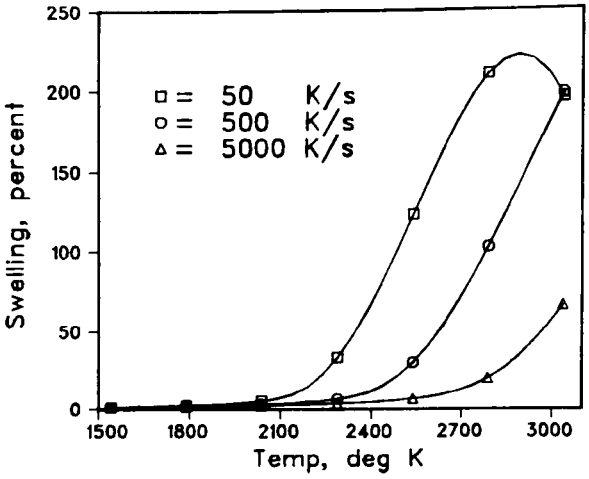

Fig. 13. FRAS-calculated Intragranular Swelling for Three Heating Rates.

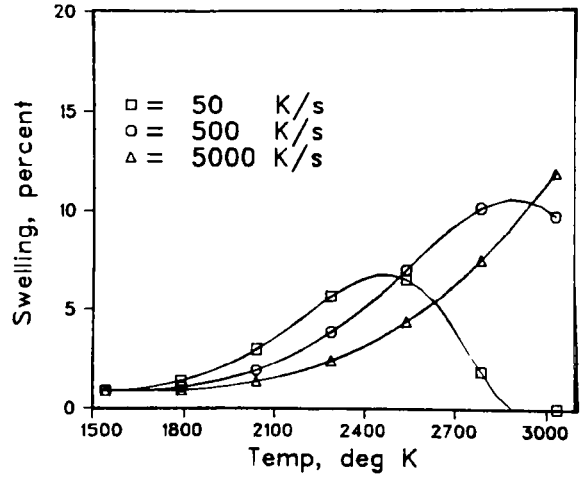

Fig. 14. FRAS2-calculated Intragranular Swelling for Three Heating Rates.

greatly as the ramp rate increases, but gross swelling is predicted even for the fastest ramp. This swelling is beyond the level at which the analysis of swelling by collisional coalescence is considered valid.[3] The decrease in swelling at higher temperatures for the slowest ramp is caused by release of gas to the grain boundaries (compare Fig. 11).

Figure 14 shows the intragranular swelling as modified by nonequilibrium effects. The fall-off in swelling occurs at lower temperatures than in the equilibrium calculations because release is more rapid, as shown in Fig. 12. The effect of thermal ramp rate is slightly less than in the FRAS calculation.

There is a fundamental difference in the swelling in the two calculations: in FRAS, swelling results directly and instantly from coalescence and temperature increases; in FRAS2, coalescence and changing temperature or pressure only provide the nonequilibrium driving force, but swelling results from equilibration or diffusion of vacancies to bubbles.

C. Dispersive Potential of Nonequilibrium Bubbles

The pressure of fission gas in intragranular bubbles is generally higher than the equilibrium pressure, due to the finite time required for bubbles to expand to the equilibrium size following coalescence or a temperature increase

during a thermal transient. This overpressured gas constitutes a source of energy that can induce fuel disruption and dispersal in some situations. The potential work that the gas can perform on the surrounding fuel can be calculated in the FRAS2 code.

The potential work that can be performed by the gas as each bubble expands to its equilibrium volume has two components: the work W done against the radial stress in the fuel, and the work required to create additional bubble surface area. The dispersive potential W can therefore be expressed as the difference between the decrease in free energy of the gas and the increase in surface energy. With the assumptions that the gas expansion is ideal, isothermal, and always at local equilibrium, the result for a given bubble is

$$W = mkT \ln (V_f/V_i) - \gamma(A_f - A_i) , \qquad (16)$$

where m is the number of gas atoms in a bubble, V is the bubble volume, and A is the surface area of the bubble. The subscripts i and f refer to initial (nonequilibrium) and final (equilibrium) states, respectively. The dispersive potential is calculated in the FRAS2 code by summing the contributions from all bubbles in a unit initial volume.

It is also of interest to characterize the range of pressures to be expected and the potential volume increase. Clearly, if the overpressure in the bubbles is small or can be relieved by a small volume change, the dispersive potential will be small. Calculations were accordingly included in the FRAS2 code to determine the overpressure, weighted according to the number of gas atoms in each bubble-size class. The volume potential has also been calculated as the difference between actual, nonequilibrium volume and the potential equilibrium volume, assuming no additional coalescence.

Application of the FRAS2 code allows a comparative evaluation of the potential for dispersive fuel motion from intragranular gas. For illustration, four cases have been considered (see Table 2): two calculated voiding-driven transients in the CRBR, corresponding to two different numerical representation of the reactor for computational purposes, and two thermal histories calculated for TREAT experiments. Although the overpressures and potential volume increases are considerably different for the two CRBR transients, the dispersive potential differs by only 10%.

Table 2. Dispersive-potential Results from FRAS2 Calculations

Case	Overpressure, MPa	Potential Volume Increase, %	Work Potential, MJ/m^3
CR/N	0.26	67	3.0
CR/A	0.15	104	2.7
F1	0.03	35	0.5
L5	0.17	27	1.2

The dispersive potentials of the TREAT experiments indicate that the L5 experiment involved considerably greater potential for fuel dispersal than the F1 experiment. Experimental results are qualitatively consistent with this result. These results are limited to consideration of the effects of intragranular gas in promoting early fuel dispersal. It must be recognized that grain-boundary separation, breakup into chunks, and even gross swelling are more likely to result directly from the effects of intergranular bubbles and pressurized porosity. However, the source of this gas is inevitably the intragranular gas.

IV. SUMMARY AND CONCLUSIONS

An explicit, although simplified, treatment of the rate of bubble equilibration has been developed. Examples have been presented to indicate conditions under which nonequilibrium is important. The FRAS2 version of the FRAS code has been developed to include this treatment of bubble equilibration. Calculations have been carried out for a variety of cases to show the response of fission gas to various transient conditions (e.g., various thermal ramp rates) when equilibration is considered. The general results of these calculations indicate a reduction in mean bubble size, an increase in intragranular bubble density, an increase in gas release to grain boundaries, and a major reduction in intragranular swelling, compared to the equilibrium results. These results are generally in agreement with expected behavior, based on experimental results, and indicate a significant improvement in modeling capability.

The greatest model difference between the FRAS and FRAS2 codes is in the calculation of intragranular swelling. In the FRAS code, bubbles were assumed to equilibrate instantly in response to coalescence or changes in temperature or pressure. Large, unrealistic changes in swelling were often predicted. In the FRAS2 code, swelling becomes a rate effect. Coalescence or changes in temperature or pressure affect only the driving force for changes in bubble volumes. Actual changes occur by the diffusion of vacancies to or from the bubbles; this is the process that we have called equilibration, and it is the only means by which swelling is altered in the FRAS2 code.

The presence of nonequilibrium bubbles in the fuel comprises a source of energy that, under some conditions, may act to disperse the fuel. The dispersive potential of the fission-gas bubbles has been quantified by considering the work that the expanding gas can perform against the stress in the material surrounding the bubble. Examples of this dispersive potential have been presented for several situations.

The work described in this report has been limited to intragranular fission-gas behavior. The behavior of fission gas after it is released to grain boundaries is expected to play a major role in the response of irradiated oxide fuel to a severe thermal transient. Work in progress will extend the present analysis to consider the effects of grain-boundary gas.

Work in progress also includes efforts to determine a "best value" for the volume-diffusion coefficient, by comparison of the experimental results with FRAS2 predictions. A major difficulty is that this coefficient can vary by two orders of magnitude at 1773 K with a change in stoichiometry from 1.94 to 1.97.[18] There is some variation in stoichiometry with both burnup and pellet radius.

ACKNOWLEDGMENTS

Helpful discussions with a number of colleagues are gratefully acknowledged. These colleagues include, but are not limited to, L. W. Deitrich, R. W. Ostensen, J. M. Kramer, R. J. DiMelfi, and G. Bandyopadhyay.

REFERENCES

1. F. A. Nichols, J. Nucl. Mat. *30*, 143-165 (1969).

2. E. E. Gruber, J. Appl. Phys. *38*, 243-250 (1967).

3. E. E. Gruber, Nucl. Tech. *35*(3), 617-634 (Oct 1977).

4. R. G. Esteves, *Fission Gas Behavior During Fast Thermal Transients*, Ph.D. Thesis, UCLA (1975).

5. J. M. Greisemeyer, W. G. Steele, D. Okrent, S. H. Chien, and A. R. Wazzan, Trans. Am. Nucl. Soc. *23*, 174 (June 1976).

6. D. Stahl and T. H. Partician, ANL-8069 (Feb 1974).

7. J. Rest, ANL-76-121, 62 (Dec 1976).

8. C. Ronchi, "Kinetics of Fission Gas and Volatile Fission-product Behavior under Transient Conditions in LWR Fuel," Appendix to ANL-75-72, *Light-Water-Reactor Safety Research Program: Quarterly Progress Report, July-September 1975.*

9. W. L. Wang and R. N. Singh, ANL, private communication (1977).

10. E. W. Greenwood, A. J. E. Foreman, and D. E. Rimmer, J. Nucl. Mat. *4*, 305-324 (1959).

11. E. E. Gruber, ANL-RDP-52, 7.18 (Oct 1976).

12. G. Bandyopadhyay, ANL-MSD, private communication (1977).

13. C. A. Hineman and O. D. Slagle, HEDL, private communications.

14. J. R. Matthews, AERE-M-2643 (Sept 1974).

15. E. E. Gruber, ANL-8134 (Nov 1974).

16. R. W. Ostensen, ANL (presently Sandia), private communication (1976).

17. D. Stahl, ANL-MSD, private communication (1976).

18. Hj. Matzke, GfK, Karlsruhe, private communication (1976).

Distribution for ANL-78-36

Internal:

J. A. Kyger
R. Avery
L. Burris
D. W. Cissel
S. A. Davis
B. R. T. Frost
D. C. Rardin
R. J. Teunis
C. E. Till
R. S. Zeno
C. E. Dickerman
H. K. Fauske
S. Fistedis
B. D. LaMar
J. F. Marchaterre
H. O. Monson
R. Sevy
A. J. Goldman
I. Bornstein
D. Rose
D. R. Ferguson
L. Baker
P. A. Lottes
L. W. Deitrich
D. H. Cho
A. E. Klickman
R. A. Noland
B. A. Korelc (3)
K. Grady (5)
T. C. Chawla
W. C. Lipinski
J. B. Heineman
C. H. Bowers
J. Hofmann
R. G. Palm
A. B. Rothman
R. Simms
D. P. Weber
H. U. Wider
A. E. Wright
W. L. Wang
E. E. Gruber (21)
R. J. DiMelfi
J. M. Kramer
T. H. Hughes
C. C. Meek
R. E. Henry
B. W. Spencer
T. E. Kraft
W. W. Marr
J. H. Tessier
D. R. Pedersen
D. H. Lennox
D. H. Thompson
G. Bandyopadhyay
M. Billone
S. Gehl
L. Neimark
R. Poeppel
J. Rest
D. Stahl
A. B. Krisciunas
ANL Contract File
ANL Libraries (5)
TIS Files (6)

External:

DOE-TIC, for distribution per UC-79p (282)
Manager, Chicago Operations Office
Chief, Chicago Patent Group
Director, DOE-RRT (2)
Director, Reactor Programs Div., CH
Director, CH-INEL
President, Argonne Universities Association
Reactor Analysis and Safety Division Review Committee:
S. Baron, Burns and Roe, Inc.
W. Kerr, U. Michigan
M. Levenson, Electric Power Research Inst.
S. Levy, S. Levy, Inc.
R. B. Nicholson, Exxon Nuclear Co., Inc.
D. Okrent, U. California, Los Angeles
N. C. Rasmussen, Massachusetts Inst. Technology